Crystal structure of magnesium chromium vanadate $Mg_2CrV_3O_{11}$, a member of the $A_2BV_3O_{11}$ vanadate family

A. Worsztynowicz and S. M. Kaczmarek
Institute of Physics, Szczecin University of Technology, Al. Piastów 48, 70-310 Szczecin, Poland

W. Paszkowicz and R. Minikayev
Institute of Physics, P.A.S., Al. Lotnikow 32/46, 02-668 Warsaw, Poland

(Received 9 March 2007; accepted 21 June 2007)

The crystal structure of recently discovered chromium (III) dimagnesium trivanadate (V) $Mg_2CrV_3O_{11}$ was refined using the Rietveld method. The crystal system of $Mg_2CrV_3O_{11}$ is triclinic with space group P_1^- ($Mg_{1.7}Zn_{0.3}GaV_3O_{11}$ type) and lattice parameters $a=6.4057(1)$ Å, $b=6.8111(1)$ Å, $c=10.0640(2)$ Å, $\alpha=97.523(1)°$, $\beta=103.351(1)°$, $\gamma=101.750(1)°$, and $Z=2$. The characteristic feature of compounds in the $A_2BV_3O_{11}$ (A=Mg,Zn and B=Ga,Fe,Cr) family is a strong tendency to share the octahedral M(1) and M(2) sites by both divalent A and trivalent B atoms, and the bipyramidal M(3) sites occupied by divalent A ions. In the present refinement, the only constraint assuming full occupancy of the M(1), M(2), and M(3) sites leads to the following Cr/(Cr+Mg) ratios: 0.70(2) at M(1), 0.24(2) at M(2), and 0.03(2) at M(3). These occupancies are discussed and compared to those of isotypic compounds. The values of interatomic distances are found to be comparable with those reported by R. D. Shannon in 1976. Electron paramagnetic resonance has been also analyzed. Two absorption lines with $g\approx2.0$ (type I) and $g\approx1.98$ (type II) have been recorded in the EPR spectra, and attributed to V^{4+} ions and Cr^{3+}–Cr^{3+} ion pairs, respectively. The exchange constant J between Cr^{3+} ions has been calculated. © *2007 International Centre for Diffraction Data.* [DOI: 10.1154/1.2770746]

Key words: magnesium, chromium, vanadium, powder diffraction, crystal structure, Rietveld refinement

I. INTRODUCTION

Multicomponent vanadates and their polymorphic modifications attract particular interest because of catalytic properties enabling their more and more widespread applications in industrial practice, e.g., as active and selective catalysts in various processes of oxidative dehydrogenation of lower alkanes (Rybarczyk *et al.*, 2001). The need for detailed understanding of catalytic properties of vanadates advocates searching for new vanadium containing materials, especially those with chains of face-sharing metal octahedra and isolated VO tetrahedra. The literature shows that there are series of compounds of a general formula $M_2FeV_3O_{11}$ in the three-component metal oxide systems of $MO-V_2O_5-Fe_2O_3$ where M=Mg, Zn (Rychlowska-Himmel and Blonska-Tabero, 1999; Wang *et al.*, 2000). The structures of $Zn_2FeV_3O_{11}$ and $Mg_2FeV_3O_{11}$ are known (Wang *et al.*, 2000). These compounds crystallize in the triclinic system and are isotypic to $Mg_{1.7}Zn_{0.3}GaV_3O_{11}$ (Müller and Müller-Buschbaum, 1992, 1993) (Table I). New ternary vanadates with comparable structures have been prepared by replacing the iron atoms in $M_2FeV_3O_{11}$ with chromium atoms. $M_2CrV_3O_{11}$ compounds in the $MO-V_2O_5-Cr_2O_3$ (M=Mg,Zn) systems have recently been synthesized (Kurzawa *et al.*, 2003a, 2003b). However, crystallographic and structural data for $Zn_2CrV_3O_{11}$ compound have yet to be determined.

Magnetic interactions and spin dynamics in the metal and ions sublattices of $M_2CrV_3O_{11}$ (M=Zn,Mg) compounds have been previously studied (Worsztynowicz *et al.*, 2005). A similarity in the values of lattice constants is observed in this vanadate family (Table I). However, metal ion distributions among the M(1), M(2), and M(3) sites depend on the compound. Two, among seven literature refinements of other $A_2BV_3O_{11}$ compounds, yield an absence of the trivalent B atoms at the M(3) site, the remaining four give a small amount (e.g., 3% to 12%) and 33% in one remaining case. In the present paper, crystal structure of polycrystalline $Mg_2CrV_3O_{11}$ is for the first time determined from high-quality powder diffraction data using Rietveld refinement.

II. EXPERIMENTAL

A. Sample preparation

$Mg_2CrV_3O_{11}$ was synthesized by solid-state reaction as follows:

$$Mg(OH)_2\cdot 3(MgCO_3\cdot H_2O)+3V_2O_5+Cr_2O_3 = 2Mg_2CrV_3O_{11}+3CO_2+4H_2O \quad (1)$$

The following reagents were used as starting materials: V_2O_5, p.a. (Riedel-de Haën, Germany), Cr_2O_3, p.a. (Aldrich, Germany), and $3\,MgCO_3\cdot Mg(OH)_2\cdot 3\,H_2O$, p.a. (POCh, Gliwice, Poland) (Kurzawa *et al.*, 2003a, 2003b). The three components were weighed in appropriate stoichiometric proportions, thoroughly homogenized by grinding, formed into pellets, and heated in air atmosphere with the following high-temperature steps: 450 °C(24 h) +550 °C(24 h)+700 °C(24 h)+720 °C(24 h). After the heating cycle, the sample was cooled to ambient temperature, ground and subjected to XRD and DTA examinations. Then they were again formed into pellets and heated, and these procedures repeated several times until homogeneous samples were obtained. The final compound

TABLE I. Structural data for known isostructural members of $A_2BV_3O_{11}$ vanadate family.

	Compound $(A_{1-x}B_x)_2CV_3O_{11}$	a [Å]	b [Å]	c [Å]	α [°]	β [°]	γ [°]	V [Å^3]	site 1	site 2	site 3	ICSD
1	$Zn_2GaV_3O_{11}$	6.449(2)	6.834(2)	9.905(6)	97.80(4)	101.89(4)	101.24(3)	411.88	$Zn_{0.67}Ga_{0.33}$	$Zn_{0.57}Ga_{0.33}$	$Zn_{0.67}Ga_{0.33}$	ICSD 72483
2	$Mg_{1.68}Zn_{0.32}GaV_3O_{11}$	6.420(3)	6.801(3)	10.009(5)	97.55(4)	102.75(4)	101.51(3)	410.57	$Mg_{0.5}Ga_{0.5}$	$Mg_{0.5}Ga_{0.5}$	$Mg_{0.68}Zn_{0.32}$	ICSD 71697
3	$Zn_2FeV_3O_{11}$	6.4538(5)	6.8393(4)	9.9924(7)	97.556(9)	102.650(8)	101.308(8)	414.93	$Zn_{1.00}$	$Zn_{0.026}Fe_{0.974}$	$Zn_{0.97}Fe_{0.026}$	ICSD 99297
4	$Zn_2FeV_3O_{11}$	6.455(1)	6.834(1)	9.988(1)	97.65(1)	102.61(1)	101.26(1)	414.53	$Zn_{0.35}Fe_{0.65}$	$Zn_{0.65}Fe_{0.35}$	$Zn_{1.00}$	ICSD 410984
5	$Mg_2FeV_3O_{11}$	6.4406(4)	6.8117(4)	10.1057(7)	97.371(8)	103.458(8)	101.504(7)	415.9	$Mg_{0.72}Fe_{0.28}$	$Mg_{0.59}Fe_{0.41}$	$Mg_{0.88}Fe_{0.12}$	ICSD 98104
6	$Mg_2FeV_3O_{11}$	6.4437(9)	6.8146(9)	10.109(1)	97.35(1)	103.45(1)	101.51(1)	415.36	$Mg_{0.55}Fe_{0.45}$	$Mg_{0.55}Fe_{0.45}$	$Mg_{0.90}Fe_{0.11}$	ICSD 98105
7	$Mg_2FeV_3O_{11}$	6.434(1)	6.806(1)	10.085(1)	97.44(1)	103.44(1)	101.56(1)	413.57	$Mg_{0.55}Fe_{0.45}$	$Mg_{0.55}Fe_{0.45}$	$Mg_{0.90}Fe_{0.10}$	ICSD 410983
8	$Mg_2CrV_3O_{11}$	6.4057(1)	6.8111(1)	10.0640(2)	97.523(1)	103.351(2)	101.750(1)	410.911	$Mg_{0.30}Cr_{0.70}$	$Mg_{0.76}Cr_{0.24}$	$Mg_{0.97}Cr_{0.03}$	This work

is brown in color and melts congruently at 900±5 °C. We have tried to grow single crystals using zone melting method but without any satisfactory results. Some physical and chemical features of the compound have already been described by Worsztynowicz *et al.* (2005), Guskos *et al.* (2004), and Guskos *et al.* (2003).

B. Diffraction measurements

The diffraction measurements were performed using a Bragg–Brentano diffractometer (PANalytical X'Pert Pro Alphal MPD), in which the Bragg–Brentano geometry was modified by the use of a Johansson (Ge) monochromator at the incident beam and a semiconductor strip detector, commercial name X'celerator, from PANalytical [this setting and its advantages are described by Paszkowicz (2005)]. The data were collected for 24 h at room temperature. Because of the X-ray optics and detector, the diffractometer produces XRD patterns with excellent statistics and quality. The equipment is well suited for XRD analysis, particularly for detecting very minor impurity phases.

The continuous scanning mode was applied. The data were recorded with $0.0167°2\theta$ steps in a broad $5°$ to $159°2\theta$ range using Cu$K\alpha_1$ radiation. The experimental parameters are summarized in Table II.

C. EPR measurements

The electron paramagnetic resonance (EPR) spectra were recorded using a Bruker E 500 X-band spectrometer ($\upsilon \sim 9.4$ GHz) with 100 kHz field modulation equipped with Oxford helium gas flow cryostat for measurements at temperatures from liquid nitrogen temperature down to 4 K. The temperature-dependent EPR spectra were collected from 4 to 300 K.

III. RESULTS

A. Rietveld refinement

Rietveld refinements (for their final result see Figure 1(a) and 1(b)) were performed using the program Fullprof 2k, version 2.50, (Rodriguez-Carvajal, 1993) for collected data from $8°$ to $159°2\theta$. The unit cell parameters of the triclinic $Mg_2CrV_3O_{11}$ are $a=6.4057(1)$ Å, $b=6.8111(1)$ Å, $c=10.0640(2)$ Å, $\alpha=97.523(1)°$, $\beta=103.351(1)°$, $\gamma=101.750(1)°$, and $Z=2$. The background was refined using the Fourier-filtering technique. Phase identification shows no impurity phases in the $Mg_2CrV_3O_{11}$ sample. The pseudo-Voigt peak shape function was used, and the shape parameters (η and x) of the profile function were refined. Correction for the effect of finite sample size on intensity at lowest angles was also included.

Other refined parameters were the scale factor, four background parameters, six lattice parameters, free positional parameters, isotropic atomic displacement parameters, three peak-width parameters, u,υ,w, sample displacement, and four parameters for profile asymmetry. The total number of refined parameters was 92. Standard deviations of refined parameters were calculated by multiplying the original standard deviations by the value of SCOR ("sigma correction")

TABLE II. Experimental parameters for XRD data collection.

Radiation	Cu$K\alpha_1$ (40 kV, 35 mA)
Wavelength (Å)	1.54060
Diffractometer radius	240 mm
Divergence slit	1°
Monochromator	Johansson (111 Ge) at the incident beam
Residual Kα_2 to Kα_1 intensity ratio	0.6%
Soller slit (incident beam)	0.02 rad
Soller slit (diffracted beam)	0.04 rad
Detector	Strip detector with full opening (127 strips, 9 mm active length corresponding to 2.1°2θ)
Angular range	5°–159°2θ, refined 8°–159°2θ
Scanning mode	Continuous scanning mode, data recorded with the step 0.0167° (2θ)
Total scanning time	24 h
Sensitivity to weak peaks at the applied collection conditions	0.2% (relative intensity)

parameter (=3.32), according to the method proposed by Bérar and Lelann (1991). The obtained unit-cell is shown in Figure 2.

In the following part of our paper, we discuss EPR results, bearing in mind the possibility of the existence of Cr^{3+}–Cr^{3+} pairs.

B. EPR results

Figure 3 shows the temperature evolution of EPR spectra for the $Mg_2CrV_3O_{11}$ compound. Two different EPR spectra dominate in the absorption spectra: wide and an intense spectrum ($g \sim 1.98$) and a weaker and narrower spectrum ($g \sim 2.0$), identified as Curves I and II in Figure 3, respectively. As the temperature increases, Curve II is not observed because it is strongly overlapped by the broad and very intense Lorentzian Curve I.

Simulation of Curve II using the *SIMPOW* program (Nilges, 1979) is in good agreement with the experimental data. Fitting results reveal small axial anisotropy with g-factors: $g_\perp = 1.973$ and $g_\parallel = 1.941$. In the entire temperature

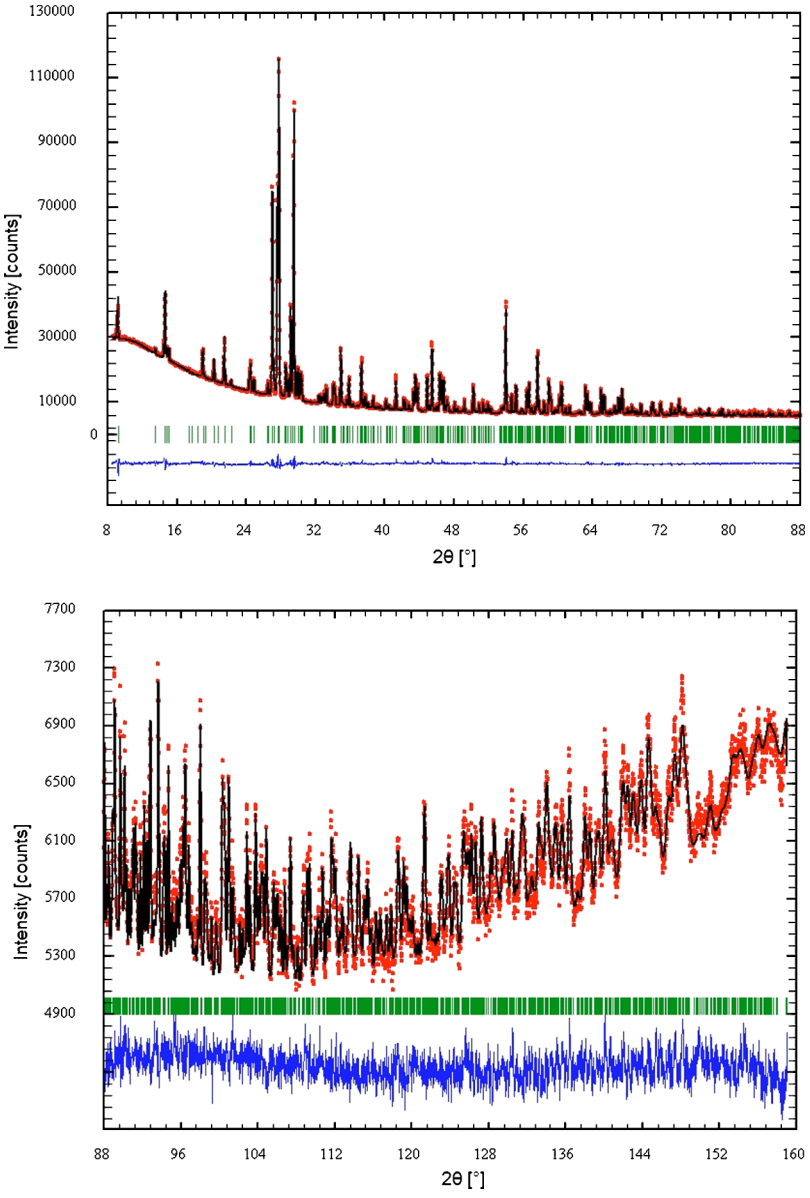

Figure 1. Rietveld refinement result for $Mg_2CrV_3O_{11}$: (a) (top) and (b) (bottom). Experimental data—red dots, calculated pattern—black solid line. The difference pattern is shown below the diffraction patterns (blue solid line). Vertical bars represent the peak positions. In order to demonstrate the fitting quality, the high-angle range is shown on a separate graph.

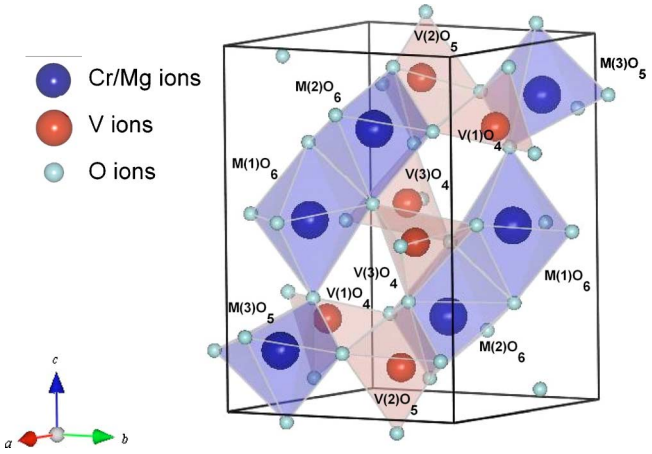

Figure 2. Unit cell of triclinic $Mg_2CrV_3O_{11}$ compound. The structure was drawn with VICS-II developed by Momma and Izumi (see http://www.geocities.jp/kmo_mma/crystal/en/vics.html).

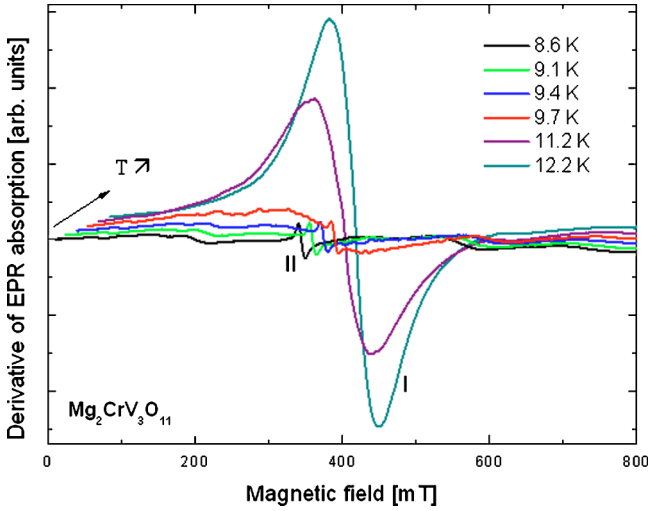

Figure 3. Temperature evolution of EPR spectra for $Mg_2CrV_3O_{11}$ compound.

range where Curve II was measured, both g-factor and peak-to-peak linewidth, $\Delta B_{eff} \approx 7$ mT, remain unchanged. The temperature dependence of the intensity of Curve II (Figure 4), obtained using double integrating of the absorption derivative, satisfies Curie law. Therefore Curve II can be attributed to V^{4+} ions or VO^{2+} centers, in good agreement with results reported by others on vanadium centers in other compounds (Gupta *et al.*, 1995; Kosava *et al.*, 2001).

Curve I with $g \sim 1.98$ can be clearly observed at higher temperatures, i.e., >15 K (not shown in Figure 3). In the temperature behavior of integral intensity of Curve II estimated by double integration of the absorption (Worsztynowicz *et al.*, 2005), a weak, but well-defined, maximum intensity at 12.2 K can be observed. Below the 16 K, I(T) decreases continuously down to lower values suggesting that some antiferromagnetic correlations are present. The specific maximum of the intensity curve and its further disappearance at low temperatures indicate the onset of a long-range AFM ordering between magnetic centers with antiparallel spin ordering. Taking into account of the intensity and peak-to-peak linewidth behavior versus temperature of Curve I (Worsztynowicz *et al.*, 2005), it could not attribute to isolated Cr^{3+} ions but to Cr^{3+} ion pairs. We have fitted the integrated intensity of the I EPR curve according to Eq. (2) (see Figure 3), where only $S=2$ total spin of interacting Cr^{3+} ions ($S=3/2$) participate in the formula of Boltzmann distribution. The expected temperature dependence of the integral EPR intensity for dimers $S=3/2$ is given by the Boltzmann law:

$$I(T)_{S=2} \propto \frac{1}{T} \frac{\exp\left(\frac{6J_{CrCr}}{kT}\right)}{1+3\exp\left(\frac{2J_{CrCr}}{kT}\right)+5\exp\left(\frac{6J_{CrCr}}{kT}\right)+7\exp\left(\frac{12J_{CrCr}}{kT}\right)}. \quad (2)$$

From the above-described fitting we can find an isotropic exchange constant, J_{CrCr} for interacting Cr^{3+}–Cr^{3+} ions, which equals $J_{CrCr}/k = -6.5(6)$ K. The accurate fitting of the experimental intensity data is shown in Figure 3.

IV. DETAILS OF RIETVELD REFINEMENT AND DISCUSSION

The starting structural model for Rietveld refinement was based on that of $Mg_2FeV_3O_{11}$ (Wang *et al.*, 2000), while the starting lattice parameters were taken from the results of indexing procedure (Kurzawa *et al.*, 2003a). The quality of the fitting, clearly demonstrated in Figures 1(a) and 1(b) leaves no doubt about the structure assignment and refined-parameters selection. The complete results on the refined $Mg_2CrV_3O_{11}$ unit-cell and R-factors are listed in Table III, and the atomic coordinates are given in Table IV.

The refinement results confirm that the $Mg_2CrV_3O_{11}$ is isostructural with $Mg_{1.7}Zn_{0.3}GaV_3O_{11}$ (Müller and Müller-Buschbaum, 1993). Magnesium and chromium atoms are found to be distributed between three different crystallographic sites: M(1) and M(2) with octahedral coordination and M(3) with trigonal bipyramidal coordination (Figure 2). Vanadium V^{5+} atoms are in the centers of edge-connected $V(2)O_5$ trigonal bipyramids and $V(3)O_4$ tetrahedrons forming $V_4O_{14}^{8-}$ cluster and an isolated $V(1)O_4$ tetrahedron [Figure 6(a)]. Each $M(3)O_5$ bipyramid shares an edge with one $M(2)O_6$ octahedron and a corner with one $M(1)_2O_{10}$ octahedral dimer [Figure 6(b)].

TABLE III. Crystallographic data for $Mg_2CrV_3O_{11}$.

Chemical formula	$Mg_2CrV_3O_{11}$
Formula weight (g/mol)	429.43
Space group	$P\bar{1}$
Wyckoff sequence	*I*17
Pearson code	*P*34
Structure type	$Mg_{1.7}Zn_{0.3}GaV_3O_{11}$
Unit cell volume (Å^3)	410.903(1)
a (Å)	6.4057(1)
b (Å)	6.8111(1)
c (Å)	10.0640(2)
α (°)	97.523(1)
β (°)	103.351(1)
γ (°)	101.750(1)
Z	2
ρ_{calc} (g·cm^{-3})	3.464
R_p [a]	1.45
R_{wp} [b]	1.9
R_{exp} [c]	1.05
R_B	6.7
R_F	5.58
χ^2	3.3
Temperature (K)	298(1)
Number of fitted parameters	92
Number of reflections for pattern	1809

[a] $R_P=\Sigma_i|I_{obs}(i)-I_{calc}(i)|/\Sigma_i(I_{obs}(i))\times 100$.
[b] $R_{wp}=(\Sigma_i(w(i)[I_{obs}(i)-I_{calc}(i)]^2/\Sigma_i(w(i)[I_{obs}(i)]^2)))^{1/2}\times 100$.
[c] $R_{exp}=((n-p)/\Sigma_i(w(i)[I_{obs}(i)]^2))^{1/2}\times 100$.

Initial Rietveld structure refinements were performed assuming the triclinic $Mg_2CrV_3O_{11}$ crystal structure with the Cr atoms confined exclusively at the M(1) sites and Mg atoms at the M(2) and M(3) sites. The distributions of the Mg and Cr atoms were established by examining the results of least-squares refinements. Full occupancies at all metal M sites were assumed. Individual Cr occupancies at these sites were not fixed during the refinements, and the Cr and Mg occupancies obtained from the final Rietveld refinement are M(1)=0.7Cr+0.3Mg, M(2)=0.24Cr+0.76Mg, and M(3) =0.03Cr+0.97Mg. The Cr:Mg ratio for this distribution is

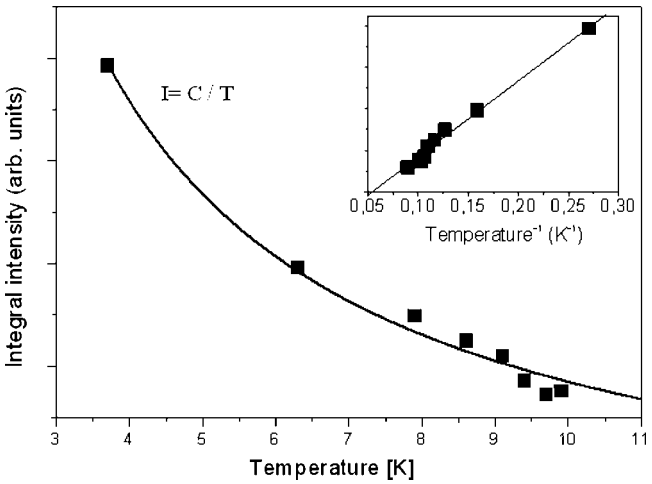

Figure 4. Temperature dependence of Curve II (squares) and fitting (solid line) according to Curie law. Inset shows reciprocal temperature dependence.

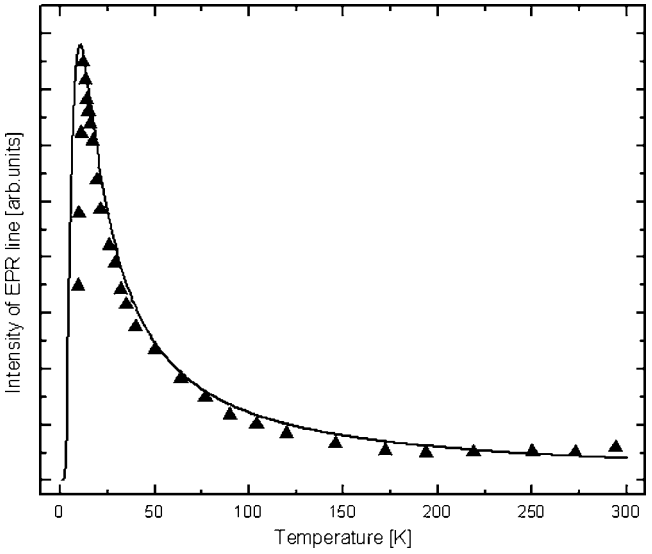

Figure 5. Temperature dependence of integral EPR intensity of Curve I and fitting results using Eq. (2).

0.97:2.03, while the expected stoichiometric ratio is 1:2. Further analysis has shown that for other starting models, [i.e., various initial distributions in the M(1), M(2), and M(3) sites] the refinement quickly converged to practically the same results. The final agreement factors reach their minima just for the result as the above. A refinement assuming a full occupancy of M(3) by Mg led to very similar structural parameters, but it also led to a still smaller Cr to Mg ratio, 0.93:2.06, instead of 0.97:2.03. Therefore, the latter model was abandoned. Table IV lists the final values of the atomic coordinates and occupancies of Mg and Cr at the M(1), M(2), and M(3) sites. We notice that the atomic displacement parameters, B_{iso}, are apparently overestimated, especially for O(3), O(4), O(11), M(2), and M(3) sites.

The $V(1)O_4$, $V(3)O_4$ tetrahedra, and $V(2)O_5$ trigonal bipyramids have V–O distances ranging from

TABLE IV. Atomic coordinates for $Mg_2CrV_3O_{11}$ and values of B_{iso}.

Atom	*x*	*y*	*z*	B_{iso}
V1	0.3299(9)	0.0143(9)	0.2122(6)	0.9(1)
V2	0.3076(9)	0.4283(9)	0.8804(6)	0.9(1)
V3	0.7407(9)	0.6713(8)	0.4672(6)	0.8(1)
O1	0.612(3)	0.131(2)	0.291(2)	0.4(4)
O2	0.250(3)	0.792(3)	0.277(2)	0.7(5)
O3	0.306(3)	0.936(3)	0.048(2)	1.1(5)
O4	0.198(3)	0.183(3)	0.847(2)	1.2(5)
O5	0.108(3)	0.559(3)	0.837(2)	0.9(4)
O6	0.841(3)	0.812(3)	0.779(2)	0.9(5)
O7	0.633(3)	0.512(2)	0.932(2)	0.7(4)
O8	0.633(3)	0.877(3)	0.514(2)	0.9(5)
O9	0.721(3)	0.474(3)	0.562(2)	0.7(4)
O10	0.612(3)	0.562(2)	0.299(2)	0.7(4)
O11	0.999(3)	0.220(3)	0.520(2)	1.3(5)
M1	0.6917(9)	0.1733(9)	0.5086(6)	0.3(2)
M2	0.763(1)	0.507(1)	0.7710(9)	1.2(3)
M3	0.176(2)	0.876(2)	0.837(1)	1.2(3)

M(1)=0.70(2)Cr+0.30(2)Mg, M(2)=0.24(2)Cr+0.76(2)Mg, M(3) =0.03(2)Cr+0.97(2)Mg.

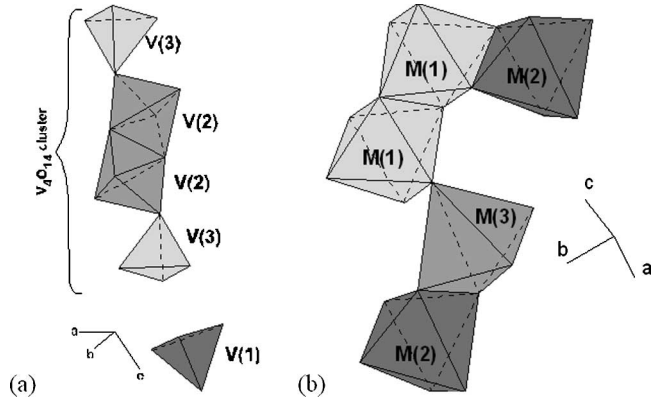

Figure 6. (a) The linkage among vanadium sites and (b) chromium/magnesium polyhedra.

1.636 to 1.777 Å, from 1.648 to 1.749 Å, and from 1.632 to 1.994 Å, respectively (Table V). They are in good agreement with those usually observed for vanadium: the mean values 1.733, 1.708, and 1.824 Å, respectively, are similar to those reported by Shannon (1976) (the V–O distance in tetrahedron is equal to 1.755 Å and in bipyramid to 1.860 Å). Such small differences between Shannon and our results could come from distortions present inside the $M(3)O_5$ bipyramid and $M(1)O_6$ and $M(2)O_6$ octahedrons.

The distribution of chromium and magnesium between the M(1), M(2), and M(3) sites can cause distortion in the geometry of $M(1)O_6$ and $M(2)O_6$ octahedra. The $M(1)O_6$ and $M(2)O_6$ octahedra exhibit M–O distances ranging from 1.904(4) to 2.099(2) Å (the mean value equals 2.011 Å) and from 1.982(4) to 2.268(4) Å (the mean value equals 2.068 Å), respectively.

TABLE V. Distances [Å] and angles (°) in the vanadium and chromium/magnesium polyhedra. M–O distances-bold numbers diagonally; O–O distances-numbers above the diagonal; O-M-O angles—numbers below the diagonal.

Isolated tetrahedr V(1)	O(1)	O(2)	O(3)	O(6)		
O(1)	**1.76(2)**	2.88(2)	2.73(2)	2.94(3)		
O(2)	110(1)	**1.76(2)**	2.70(3)	2.97(3)		
O(3)	107(1)	105(2)	**1.64(2)**	2.75(3)		
O(6)	112(2)	115(2)	107(2)	**1.78(2)**		
Trigonal bipyramid V(2)	O(4)	O(5)	O(7)	$O(7)^i$	$O(10)^i$	
O(4)	**1.63(2)**	2.75(3)	3.06(2)	2.68(2)	2.70(3)	
O(5)	111(2)	**1.71(2)**	3.37(3)	2.70(3)	2.68(3)	
O(7)	116(1)	132(1)	**1.97(2)**	2.42(3)	2.41(2)	
$O(7)^i$	102(2)	100(1)	79(1)	**1.81(2)**	3.70(3)	
$O(10)^i$	96(2)	93(1)	75(1)	153(1)	**1.99(2)**	
Tetrahedr V(3)	O(8)	O(9)	O(10)	O(11)		
O(8)	**1.74(2)**	2.99(3)	2.80(2)	2.66(3)		
O(9)	118(2)	**1.75(2)**	2.76(3)	2.80(3)		
O(10)	109(2)	106(2)	**1.70(2)**	2.73(2)		
O(11)	157(2)	43(1)	91(1)	**1.65(2)**		
Octahedr Cr/Mg(1)	O(1)	$O(2)^i$	O(8)	$O(8)^i$	O(9)	O(11)
O(1)	**2.10(2)**	4.17(2)	3.00(3)	2.78(3)	3.20(2)	2.87(2)
$O(2)^i$	177(1)	**2.07(2)**	2.73(2)	2.89(2)	2.59(3)	2.87(3)
O(8)	95(1)	84(1)	**1.99(2)**	2.62(3)	3.94(3)	2.94(3)
$O(8)^i$	86(1)	91(1)	82(1)	**1.99(2)**	2.82(2)	3.89(3)
O(9)	102(1)	79(1)	161(2)	90(1)	**2.01(2)**	2.79(3)
O(11)	91(1)	92(2)	98(1)	177(2)	90(2)	**1.90(2)**
Octahedr Cr/Mg(2)	$O(2)^i$	O(5)	O(6)	O(7)	O(9)	$O(10)^i$
$O(2)^i$	**2.01(2)**	2.85(2)	3.98(3)	3.08(3)	2.59(3)	3.04(3)
O(5)	88(1)	**2.10(2)**	2.69(3)	3.37(3)	3.15(2)	4.36(2)
O(6)	162(2)	81(1)	**2.02(2)**	2.99(3)	2.80(2)	3.31(2)
O(7)	101(2)	111(2)	97(1)	**1.98(2)**	3.87(3)	2.41(2)
O(9)	80(1)	100(1)	87(1)	149(2)	**2.03(2)**	2.79(3)
$O(10)^i$	90(1)	178(1)	101(1)	69(1)	81(1)	**2.27(2)**
Trigonal bipyramid Cr/Mg(3)	$O(1)^i$	O(3)	O(4)	O(5)	O(6)	
$O(1)^i$	**2.08(3)**	3.55(3)	3.01(3)	3.09(3)	3.69(3)	
O(3)	119(1)	**2.04(2)**	2.84(3)	2.95(2)	3.40(2)	
O(4)	93(1)	88(1)	**2.05(2)**	4.15(3)	2.93(2)	
O(5)	95(1)	91(1)	171(1)	**2.11(2)**	2.69(3)	
O(6)	128(2)	113(1)	92(1)	81(1)	**2.03(2)**	

Symmetry code: x, y, z; (i) $-x, -y, -z$

In the latter case, where the M(2) positions are occupied mainly by magnesium (76%), the magnesium higher effective ionic radius could be a reason for larger difference in M–O distances. It is common knowledge that Cr^{3+} ion has the highest octahedral site preference of all the 3d metals (69 kJ/mol) (Weiss and Witte, 1983), and this could partially explain the missing of the Cr ions at fivefold coordination of the M(3) site position. The Mg–O distances in the $Mg(3)O_5$ trigonal bipyramids are ranging from 2.028 to 2.110 Å (the mean value equals 2.062 Å) and are in good agreement with those usually observed (=2.06 Å) (Shannon, 1976) for Mg ions in fivefold coordination.

V. CONCLUSIONS

$Mg_2CrV_3O_{11}$ has been found to crystallize in triclinic symmetry (space group P_1^-) with lattice parameters a =6.4057(1) Å, b=6.8111(1) Å, c=10.0640(2) Å, α =97.523(1)°, β=103.351(1)°, γ=101.750(1)°, and Z=2. It is isotypic to $Mg_{1.7}Zn_{0.3}GaV_3O_{11}$. Cr^{3+} and Mg^{2+} ions are mixed and located at the centers of $M(1)O_6$ and $M(2)O_6$ octahedra and one $M(3)O_5$ bipyramid. The distributions of the Cr^{3+} and Mg^{2+} ions at the M(1), M(2), and M(3) sites are M(1)=0.70Cr+0.30Mg, M(2)=0.24Cr+0.76Mg, and M(3) =0.03Cr+0.97Mg. As for other compounds in this family, a small fraction of transition metal at the M(3) site is found. Although this occupancy is here only slightly larger than the standard deviation, this kind of behavior seems to be a rule in these materials.

The values of V–O distances in the vanadium polyhedra found in this study are typical for vanadium ions: The mean values we observed are 1.733 and 1.708 Å for tetrahedral coordination and 1.824 Å for fivefold coordination. The mean value of Mg–O distance in the $Mg(3)O_5$ polyhedra is equal to 2.062 Å and is in good agreement with those reported (=2.06 Å) for Mg ions in this coordination. The geometry of the $M(1)O_6$ and $M(2)O_6$ octahedra shows significant distortions attributable to distribution of chromium and magnesium ions between the M(1) and M(2) sites.

Based on the above structural consideration it can be concluded that Cr^{3+} ions may form effective pairs at the M(1) sites, forming $M(1)_2O_{10}$ octahedral dimers. EPR spectra of these Cr^{3+}–Cr^{3+} dimers have been observed. The fitting of the intensities of the EPR curve shows that Cr^{3+} dimers are antiferromagnetically coupled with the exchange constant being equal to J_{CrCr}/k=−6.5(6) K.

ACKNOWLEDGMENTS

The authors thank Professor Jolanta Kurzawa and Dr. Monika Bosacka from the Department of Inorganic and Analytical Chemistry, Szczecin University of Technology, Poland, for the preparation of $Mg_2CrV_3O_{11}$.

Bérar, J.-F. and Lelann, P. (**1991**). "E.S.D.'s and Estimated Probable Error Obtained in Rietveld Refinements With Local Correlations," J. Appl. Crystallogr. **24**, 1–5.

Gupta, S., Khanijo, N., and Mansingh, A. (**1995**). "The Influence of V^{4+} Ion Concentration on the EPR Spectra of Vanadate Glasses," J. Non-Cryst. Solids **181**, 58–63.

Guskos, N., Wabia, M., Kurzawa, M., Beskrovnyj, A., Likodimos, V., Typek, J., Rychlowska-Himmel, I., and Blonska-Tabero, A. (**2003**). "Neutron Diffraction Study of $Mg_2FeV_3O_{11-\delta}$," Radiat. Eff. Defects Solids **158**, 369–374.

Guskos, N., Typek, J., Beskrovnyj, A., Wabia, M., Kurzawa, M., Anagnostakis, E. A., and Gasiorek, G. (**2004**). "Neutron Studies of Cation Disorder in $Zn_2FeV_3O_{11-\delta}$," J. Alloys Compd. **377**, 47–52.

Kosava, N. V., Vosel, S. V., Anufrienko, V. F., Vasenin, N. T., and Devyatkina, E. T. (**2001**). "Reduction Processes in the Course of Mechanochemical Synthesis of $Li_{1+x}V_3O_8$," J. Solid State Chem. **160**, 444–449.

Kurzawa, M., Rychlowska-Himmel, I., Bosacka, M., and Dabrowska, G. (**2003a**). "A New Compound $Mg_2CrV_3O_{11}$ and Phase Relations in the MgV_2O_6–$MgCr_2O_4$ System in the Solid State," Solid State Phenom. **90–91**, 353–358.

Kurzawa, M., Rychlowska-Himmel, I., Blonska-Tabero, A., Bosacka, M., and Dabrowska, G. (**2003b**). "Synthesis and Characterization of New Compounds $Ni_2CrV_3O_{11}$ and $Zn_2CrV_3O_{11}$," Solid State Phenom. **90–91**, 347–352.

Müller, C. and Müller-Buschbaum, Hk. (**1992**). "Zur Kenntnis von $Mg_{2-x}Zn_xGaV_3O_{11}$ (x=0,3)," J. Alloys Compd. **185**, 163–168.

Müller, C. and Müller-Buschbaum, Hk. (**1993**). "Zur Kenntnis von $Zn_2GaV_3O_{11}$," J. Alloys Compd. **191**, 251–253.

Nilges, M. J. (**1979**). "Electron Paramagnetic Resonance Studies of Low Symmetry Nickel(I) and Molybdenum(V) Complexes," Ph.D. dissertation, University of Illinois, Urbana, Illinois.

Paszkowicz, W. (**2005**). "Application of a Powder Diffractometer Equipped with a Strip Detector and Johansson Monochromator to Phase Analysis and Structure Refinement," Nucl. Instrum. Methods Phys. Res. A **551**, 162–177.

Rodríguez-Carvajal, J. (**1993**). "Recent Advances in Magnetic Structure Determination by Neutron Powder Diffraction," Physica B **192**, 55–69.

Rybarczyk, P., Berndt, H., Radnik, J., Pohl, M., Buyevskaya, O., Baerns, M., and Bruckner, A. (**2001**). "The Structure of Active Sites in *Me*-V–O Catalysts (*Me*=Mg,Zn,Pb) and Its Influence on the Catalytic Performance in the Oxidative Dehydrogenation (ODH) of Propane," J. Catal. **202**, 45–58.

Rychlowska-Himmel, I. and Blonska-Tabero, A. (**1999**). "Studies on the System ZnO–V_2O_5–Fe_2O_3 Reactivity of $ZnFe_2O_4$ towards ZnV_2O_6," J. Therm Anal. Calorim. **56**, 205–210.

Shannon, R. D. (**1976**). "Revised Effective Ionic Radii and Systematic Studies of Interatomic Distances in Halides and Chalcogenides," Acta Crystallogr., Sect. A: Cryst. Phys., Diffr., Theor. Gen. Crystallogr. **32**, 751–767.

Wang, X., Vander Griend, D. A., Stern, Ch. L., and Poeppelmeier, K. R. (**2000**). "Structure and Cation Distribution of New Ternary Vanadates $FeMg_2V_3O_{11}$ and $FeZn_2V_3O_{11}$," J. Alloys Compd. **298**, 119–124.

Weiss, A. and Witte, H. (**1983**). *Kristallstrukture und Chemische Bindung* (Verlag Chemie, Weinheim).

Worsztynowicz, A., Kaczmarek, S. M., Kurzawa, M., and Bosacka, M. (**2005**). "Magnetic Study of Cr^{3+} Ion in $M_2CrV_3O_{11-x}$ (M=Zn,Mg) Compounds," J. Solid State Chem. **178**, 2231–2236.